

## Is Water Templating Nanoporous Materials?

Marc Henry,<sup>\*[a]</sup> Francis Taulelle,<sup>[a]</sup> Thierry Loiseau,<sup>[b]</sup> Lionel Beitone,<sup>[b]</sup> and Gerard Férey<sup>[b]</sup>

**Abstract:**  $(\text{H}_2\text{O})_{17}$ , a cluster with pentagonal water arrangements, squeezed in the sodalite cage of the crystal structure MIL-74 ( $\text{Zn}_6\text{Al}_{12}\text{P}_{24}\text{O}_{96} \cdot [\text{N}(\text{CH}_2\text{CH}_2\text{NH}_3)_3]_8 \cdot (\text{H}_2\text{O})_{34}$ ), has its oxygen atoms well located by X-ray powder diffraction. Positioning of hydrogen atoms has been performed by a dynamic partial atomic charges and hardnesses analysis calculation, in

which partial charges are recalculated for each hydrogen sub-network modification. Hydrogen atoms are therefore positioned by energy minimization. A quantitative estimation of the hydrogen

bonds energy for each H–bond and for the network in the MIL-74 nanoporous compound has been obtained. This result allows a discussion of the effect of imprinting the nanoporous structure onto water or alternatively the templating effect of the cluster onto the inorganic framework.

**Keywords:** clathrates • nanoporous materials • templating effect • water chemistry • water structure

### Introduction

The MIL-74 structure ( $\text{Zn}_6\text{Al}_{12}\text{P}_{24}\text{O}_{96} \cdot [\text{N}(\text{CH}_2\text{CH}_2\text{NH}_3)_3]_8 \cdot (\text{H}_2\text{O})_{34}$ )<sup>[1]</sup> is quite a special compound that may be viewed as a super-sodalite network with  $\text{Al}[\text{Zn}_2\text{Al}_2\text{P}_4\text{O}_{24}]$  super-square units (Figure 1). This is a beautiful example of 'scaled chemistry' in the sense of G. Férey<sup>[2]</sup> or of 'decoration of the sodalite network' in the sense of M. O'Keeffe.<sup>[3]</sup> This structure has the lowest framework density known to date, in which the cationic templates ( $\text{TREN} = [\text{N}(\text{CH}_2\text{CH}_2\text{NH}_3)_3]^{3+}$ ) are included as part of the framework and cover the hexagonal pores of the sodalite cage. The use of organic molecules as templating agents is widespread in zeolite synthesis.<sup>[4]</sup> Templating fulfils a triple role by directing the structure, controlling the shape, and fixing the basicity of the synthesis.<sup>[5]</sup> If selectivity between the templating agent and the framework has been established in the case of the ZSM-18 zeolite,<sup>[6]</sup> it is likely that many other frameworks may be synthesized without such selectivity. The interplay between

the different roles of the templating agent appears to leave sufficient room for such flexibility. It also suggests, among several possibilities that are close in energy, yet another hidden partner that could be responsible for the selection of the finally observed structure.

Accordingly, even if TREN cations obstruct the channels, they nevertheless leave the pore cavity accessible to water molecules. This leads to the other exceptional feature of this structure, that is, the occurrence of a highly symmetrical water cluster comprising 17 water molecules located in the sodalite cage and organized in an amazingly well-defined pattern of pentagons.<sup>[1]</sup> Determination, by diffraction, of the number and the nature of the structure of the water clusters in the pores of nanoporous structures is a challenging issue, owing to both static and motional disorder. Consequently, the water network has only been determined accurately for very few materials. The structure of bound water in VPI-5 has been successfully determined at low temperature, and shows an exceptional water-based triple helix.<sup>[7]</sup> The MIL-74 structure is therefore quite instructive with its very well-defined aggregate of seventeen water molecules. This observation raises the interesting question of the role played by water molecules during crystal nucleation and growth. In most advanced efforts of template design for a better selectivity,<sup>[8]</sup> water is never considered as a possible template. It is supposed, at best, to play the role of a void-filling agent. With this contribution we aim to show that this last view is far too restrictive, and to open the discussion on the templating role of water.

[a] Prof. M. Henry, Dr. F. Taulelle  
Tectonique Moléculaire du Solide, UMR CNRS 7140  
Université Louis Pasteur  
4 Rue Blaise Pascal, 67070 Strasbourg Cedex (France)  
E-mail: henry@chimie.u-strasbg.fr

[b] Dr. T. Loiseau, Dr. L. Beitone, Prof. G. Férey  
Institut Lavoisier, UMR CNRS 8637  
Université de Versailles St Quentin en Yvelines  
45 Avenue des Etats-Unis  
78035 Versailles Cedex (France)

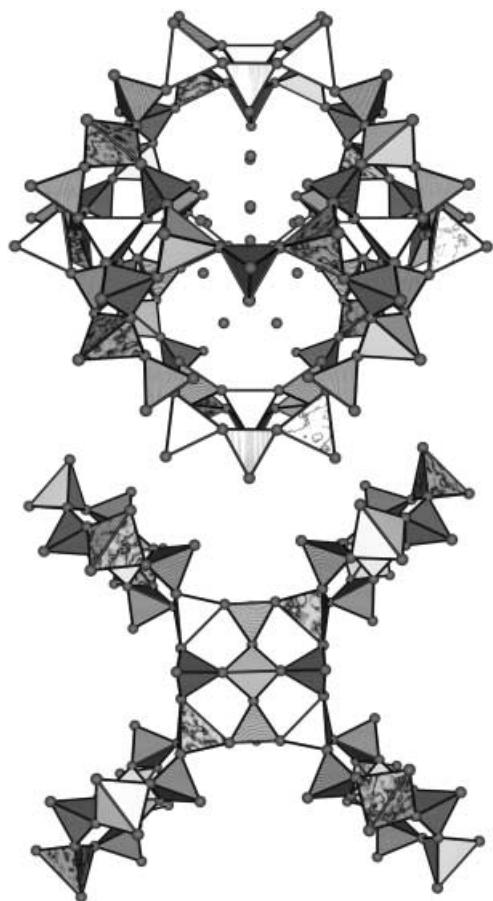


Figure 1. The MIL-74 structure with its  $O_{17}$  cluster (isolated atoms) encapsulated into a sodalite cage (top) decorated with  $Al[Zn_2Al_2P_4O_{24}]$  square units (bottom). Surface effect code: Al gray, P wood, Zn marble, O black.

## Method

Unraveling the role of water as a templating agent is not possible without knowing accurately the positions of the H atoms. As shown in Figure 1, the positions of the H atoms are scarcely determined in X-ray diffraction experiments. Consequently, structural features of such structures are commonly discussed in terms of the framework atoms only. A fast and reliable way to get these crucial coordinates from X-ray data is to rely on the nonempirical version of the partial atomic charges and hardnesses analysis (PACHA).<sup>19,10</sup> For the actual calculation of the water cluster of MIL-74, the structural data have to be formatted to ensure good convergence of the lattice sums procedures. In PACHA this is done by the systematic use of symmetry masks to handle disordered situations, and after minimization of the lattice energy this leads to optimized values for the coordinates of the H atoms. Templates and associated water molecules are therefore fully localized, with the “heavy” and “light” atoms in place, complete energy computations are then possible.

MIL-74 can be described in both the  $I\bar{4}3m$  and  $P\bar{4}3n$  space groups, with Zn and Al disordered on the same 12d site in  $I\bar{4}3m$  and ordered in 6c and 6d 2b sites in  $P\bar{4}3n$ . For simplicity of the calculation, only the ordered case  $P\bar{4}3n$  has been considered. However, even with this choice, some ad-

ditional formatting must be performed. The disorder that affects the carbon atoms of the TREN cation is handled by discarding either the C1 or the C11 position from the original structure data file. Making the C1 choice fixes the N–C and C–C distances at 148 and 153 pm, respectively, whereas making the C11 choice fixes the same distances at 147 and 154 pm. As these are very minute differences, we have arbitrarily retained the C1 position for this study. Having made this initial choice, two H atoms have been added at each carbon atom by constraining all C–H distances at 107.3 pm and all H–C–H bond angles at 109°. For the  $NH_3$  group, N–H bond lengths were fixed at 101 pm and C–N–H or H–N–H bond angles were fixed at 110° (tetrahedral geometry around nitrogen). Two dihedral angles were also kept fixed at  $\pm 120^\circ$ , the last one being allowed to take any arbitrary value between 0 and 360°. One H atom was added to atom O1W (O–H bond length fixed at 97 pm) displaying 23 point group symmetry using the [12.5.8...] symmetry mask in order to get the right  $(H_2O)_2$  stoichiometry. In this notation, a dot at position # $n$  ( $1 \leq n \leq 48$ ) means that the associated symmetry operation of the space group  $P\bar{4}3n$  is not applied during the generation of the unit cell. Conversely, the occurrence of a digit at position # $n$  refers to the ordinal number of the Seitz matrix that must be applied to get the full generation of a point in the given space group. The correspondence between these ordinal numbers  $n$  and their associated Seitz matrices is given in the CIF file provided as Supporting Information. For the O2W position displaying 3 point group symmetry, two H atoms were added with two O–H bond lengths fixed at 97 pm, and one H–O–H bond angle fixed at 105° using a [123.56.8.10.12...] symmetry mask. The three remaining torsion angles were arbitrarily varied. Similar O–H bond lengths and H–O–H bond angles with three adjustable torsion angles were used for the O3W atom. The full  $P\bar{4}3n$  space group symmetry was applied to these two H atoms bonded to a general position. The above model thus defines a 7-vertices simplex that allows us to look for a minimum of the corresponding lattice energy. This procedure converged after 386 iterations towards a minimum value of the electrostatic balance (EB) of  $-49419.8 \text{ kJ mol}^{-1}$  with a maximum value spotted at  $-46460.5 \text{ kJ mol}^{-1}$ .

A simplex optimization procedure has also been applied to the  $(H_2O)_{17}$  water cluster isolated from its crystalline environment. For the 16 outer O atoms, two H atoms have been added, constraining the two O–H bond lengths at 97 pm and the H–O–H bond angle to 105°. The H–O–H bond angle for the remaining central water molecule was set to 109.5° instead of 105° owing to its obvious tetrahedral symmetry. A 51-vertices simplex was thus defined for the 51 remaining torsion angles that were varied arbitrarily. The electrostatic balance for this free cluster was observed to converge towards  $-3718.4 \text{ kJ mol}^{-1}$  after 15591 iterations, with a maximum value at  $-2934.1 \text{ kJ mol}^{-1}$ .

The atomic coordinates generated by this calculation are available as a CIF file in the Supporting Information. From these coordinates it becomes easy to determine for each hydrogen bond the angle existing between the O–H bond and the O–O direction, for both the cluster encapsulated in the crystal and the “free” or “relaxed” cluster without interac-

tions with the inorganic framework. This crucial information can then be most easily visualized by using a histogram representation from which a statistical analysis may be easily performed. Our model, however, also provides us with direct access to the associated H–bond energy and allows us to visualize how the mean H–bond energy is partitioned between the various geometrical situations. These H–bond energies are derived after the evaluation of the electrostatic balances for meaningful molecular fragments isolated from the crystal or the molecule. As described in earlier work,<sup>[9,10]</sup> these EB values correspond to absolute formation enthalpies that depend only on the spatial disposition of the atoms in the molecular or crystalline structure. They can be used in accord with the Hellman–Feynman theorem,<sup>[11]</sup> which allows one to split the total energy into an approximately constant quantum contribution  $F$  (ruled by chemically bonded atoms) and a structure-dependent electrostatic one  $EB$  (ruled by spatial disposition of non-chemically bonded atoms). Therefore, for any system  $S$ , which is in a frozen geometry and considered to be derived from the association of two subsystems  $A$  and  $B$ , the quantity  $E_{AB} = EB(S) - [EB(A) + EB(B)]$  was shown<sup>[9]</sup> to characterize their interaction energy in a nonempirical way. In the present case, H-bond energies were obtained by using the following general automated procedure:

- 1) Selection of a threshold  $d[\text{H}\cdots\text{O}]_{\text{max}}$  distance below which a given H atom will be considered as being H-bonded to a neighboring oxygen atom. For ice-poly-morphs a typical value is  $d[\text{H}\cdots\text{O}]_{\text{max}} = 180$  pm, whereas for water clusters buried at the heart of A. Müller's superfullerene keplerates, a higher value ( $d[\text{H}\cdots\text{O}]_{\text{max}} = 200$  pm) has to be considered.<sup>[10]</sup>
- 2) Attachment to the selected H atom of its two associated O atoms: the O-donor directly bonded at  $d_{\text{OH}} < 100$  pm and the O-acceptor H-bonded at  $d_{\text{OH}} < d[\text{H}\cdots\text{O}]_{\text{max}}$ .
- 3) Attachment to these two O atoms of their chemically bonded H atoms ( $d_{\text{OH}} < 100$  pm), which define an isolated dimer  $(\text{H}_2\text{O})_2$ . Application of the PACHA formalism to this free dimer leads to a first EB value ( $EB_{\text{dim}}$ ).
- 4) Two other EB values ( $EB_{\text{donor}}$  and  $EB_{\text{acceptor}}$ ) may then be derived after separation of the two water molecules forming the previous dimer.
- 5) A residual negative interaction energy may then be readily evaluated as:  $E_{\text{res}} \sim EB_{\text{dim}} - (EB_{\text{donor}} + EB_{\text{acceptor}})$  that may be identified, according to the Hellman–Feynman theorem, to a characteristic H–bond energy.

The detailed results on a per H bond basis obtained by applying this procedure to both the free cluster and the encapsulated cluster are reported in the Supporting Information. Associated histograms are visualized in Figure 2. Such a procedure is not only limited to dimeric species but higher polymers may be also considered. Here, a mean hydrogen-bond energy  $\langle E_{\text{HB}} \rangle$  may be computed by comparing the electrostatic balance of a cluster containing  $n$  water molecules ( $EB_n$ ) to the sum of the EB values that characterize the  $n$  isolated water molecules ( $EB_i$ ). With this rigorous mathematical definition of the interaction energy,  $\langle E_{\text{HB}} \rangle$

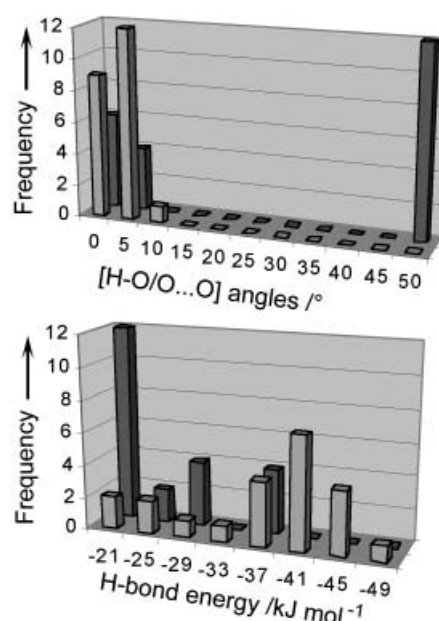


Figure 2. Hydrogen-bond angle distribution (top) and hydrogen-bonds energy distribution (bottom) for two water clusters derived from the same  $\text{O}_{17}$  atomic core found in the crystal structure of MIL-74. The data in the foreground refer to a completely free relaxed cluster, while the data in the background is related to the cluster encapsulated within the crystalline network.

$= (EB_n - \sum_i EB_i) / n$ , the supramolecular building scheme of the cluster may be unveiled (without any a priori knowledge) from the smallest possible scale (dimers) up to the largest one (whole cluster or full network). Some of these EB values for some meaningful fragments that may be identified in these clusters are given in Table 1.

Table 1. Electrostatic balances computed (with PACHA) for the various H–bonds geometry studied in this work.

Balance	Fragment	H-bonds	Status	EB [kJ mol <sup>-1</sup> ]
EB <sub>1</sub>	FT <sub>8</sub> W <sub>34</sub>	68	Zn <sub>6</sub> Al <sub>12</sub> P <sub>24</sub> O <sub>96</sub> (TREN) <sub>8</sub> (H <sub>2</sub> O) <sub>34</sub>	-49 419.8
EB <sub>2</sub>	F	0	empty Zn <sub>6</sub> Al <sub>12</sub> P <sub>24</sub> O <sub>96</sub> net	-39 256.2
EB <sub>3</sub>	FT <sub>8</sub>	24	Zn <sub>6</sub> Al <sub>12</sub> P <sub>24</sub> O <sub>96</sub> (TREN) <sub>8</sub>	-42 640.7
EB <sub>4</sub>	FW <sub>34</sub>	44	Zn <sub>6</sub> Al <sub>12</sub> P <sub>24</sub> O <sub>96</sub> (H <sub>2</sub> O) <sub>34</sub>	-46 092.0
EB <sub>5</sub>	(H <sub>2</sub> O) <sub>17</sub>	22	trapped	-32 692.2
EB <sub>6</sub>	TREN	0	trapped	-341.0
EB <sub>7</sub>	H <sub>2</sub> O	0	$\theta_{\text{H}\cdots\text{O}\cdots\text{H}} = 105^\circ$	-171.3
EB <sub>8</sub>	H <sub>2</sub> O	0	$\theta_{\text{H}\cdots\text{O}\cdots\text{H}} = 109.5^\circ$	-174.4
EB <sub>9</sub>	(H <sub>2</sub> O) <sub>2</sub>	2	$d_{\text{OO}} = 254$ pm	-365.3
EB <sub>10</sub>	(H <sub>2</sub> O) <sub>3</sub>	2	$d_{\text{OO}} = 263$ pm	-581.1
EB <sub>11</sub>	(H <sub>2</sub> O) <sub>3</sub>	2	$d_{\text{OO}} = 276$ pm	-566.5
EB <sub>12</sub>	(H <sub>2</sub> O) <sub>17</sub>	22	relaxed	-37 184.4
EB <sub>13</sub>	H <sub>2</sub> O	0	$\theta_{\text{H}\cdots\text{O}\cdots\text{H}} = 109.5^\circ$	-180.1
EB <sub>14</sub>	(H <sub>2</sub> O) <sub>2</sub>	1	$d_{\text{OO}} = 254$ pm	-389.6
EB <sub>15</sub>	(H <sub>2</sub> O) <sub>2</sub>	1	$d_{\text{OO}} = 263$ pm	-378.5
EB <sub>16</sub>	(H <sub>2</sub> O) <sub>2</sub>	1	$d_{\text{OO}} = 276$ pm	-380.0
EB <sub>17</sub>	(H <sub>2</sub> O) <sub>5</sub>	4	$d_{\text{OO}} = 276$ pm	-962.0
EB <sub>18</sub>	H <sub>2</sub> O	0	hexagonal ice	-159.8
EB <sub>19</sub>	(H <sub>2</sub> O) <sub>5</sub>	4	ice I <sub>h</sub> ( $d_{\text{OO}} = 275$ pm)	-896.8

## Discussion

It is known from neutron diffraction data that water in mesoporous cavities (2–50 nm) shows significant modifications

in its structural characteristics from water in the bulk phase.<sup>[11]</sup> Basically, the confinement of water at a nanometer scale leads to a denser H-bond network which depresses the nucleation temperature and favors formation of the cubic ice polymorph.<sup>[12]</sup> In the liquid state, the behavior of confined water was shown to be similar to that of supercooled water at lower ( $\sim 30$  K) temperature.<sup>[13]</sup> For pore sizes smaller than 2 nm, one may expect a more drastic change owing to the competition for H-bonding between water molecules and H-bonding with the walls of the confining material. A clear understanding of this interaction regime will be obviously of considerable interest as such pore sizes are commonly generated not only during zeolite nucleation but also during protein folding for instance. Although numerous theoretical studies<sup>[14–16]</sup> have been devoted to the study of small water clusters  $(\text{H}_2\text{O})_n$  ( $n < 10$ ), none of them were concerned with the structural response of large assemblies of water molecules ( $n > 10$ ) confined below the 2 nm scale. With realistic H-bond patterns obtained by PACHA, we are now in a position to address some fundamental issues raised by the existence of water clusters trapped inside nanoporous materials:

- 1) What is the order of magnitude of the interaction energy between the template and the framework?
- 2) How the H-bond pattern between water molecules changes when an otherwise encapsulated cluster is freed from its crystalline environment?
- 3) Is there any change in H-bond strength associated to the encapsulation or the release process?

Let us first deal with the template and its predicted H-bond geometry at the  $\text{EB}_1$  minimum (Figure 3). A quite regular and easily anticipated intramolecular pattern of 12 H bonds is formed, which demonstrates the validity of our method. The order of magnitude of the mean H-bond energy associated to this 12 N–H $\cdots$ O H-bond pattern may be estimated from Table 1. As stated above, we just have to compare the  $\text{EB}$  values of the TREN cations ( $8 \times \text{EB}_6$ ) and of the empty network ( $\text{EB}_2$ ) to the  $\text{EB}_3$  value that characterizes a templated network displaying empty sodalite cages:  $E_{\text{HB}} = (\text{EB}_3 - (8 \times \text{EB}_6) + \text{EB}_2) / (12 \times 8) = -6.8 \text{ kJ mol}^{-1}$ . As expected this value is found to be intermediate between van der Waals interactions (less than  $-4 \text{ kJ mol}^{-1}$ ) and O–H $\cdots$ O interactions (about  $-20 \text{ kJ mol}^{-1}$ ).

Interestingly enough, such unsurprising obvious considerations do not apply to the water clusters trapped inside the sodalite cages. As explained in the Method section, Figure 2 displays the distribution of H-bond angles and H-bond energies for two clusters sharing the same  $\text{O}_{17}$  backbone. The first  $(\text{H}_2\text{O})_{17}$  geometry was obtained when considering the cluster placed inside a crystalline lattice displaying the  $P\bar{4}3n$  space group symmetry. As far as H-bond angles are concerned, it is characterized by a striking bimodal distribution, with a first set characterized by  $\theta(\text{H}-\text{O}\cdots\text{O}) < 5^\circ$  and a second set displaying much wider values  $\theta(\text{H}-\text{O}\cdots\text{O}) \approx 50^\circ$ . As shown in the bottom part of Figure 2, these large angles are clearly associated with the less stable hydrogen bonds ( $E_{\text{HB}} \sim -21 \text{ kJ mol}^{-1}$ ). Another interesting feature lies in the

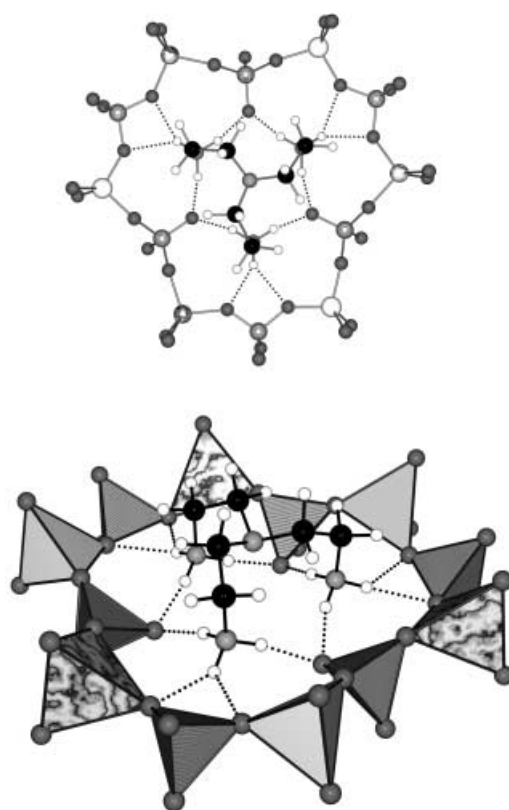


Figure 3. Predicted H-bond geometry (12H bonds with  $E_{\text{HB}} = -6.8 \text{ kJ mol}^{-1}$ ) for the TREN cation spanning the 12-ring pore of the sodalite structure. Top: front view using ball-and-sticks representation. Bottom: polyhedral side view (surface effect code: Al gray, P wood, Zn marble, O black).

bimodal distribution ( $-25 < E_{\text{HB}} < -30 \text{ kJ mol}^{-1}$  and  $E_{\text{HB}} \sim -37 \text{ kJ mol}^{-1}$ ) of the H-bond energies within the first set characterized by  $\theta(\text{H}-\text{O}\cdots\text{O}) < 5^\circ$ . It is then obvious that we were not able in this case to recover the naive image obtained by merely drawing straight lines among O atoms located less than 300 pm apart (bottom left of Figure 4). As indicated by the two histograms in the rear of Figure 2, this cluster displays its own supramolecular architecture dictated by the presence of the inorganic framework. As a whole, the cluster has 22 hydrogen bonds with a mean H-bond energy readily evaluated as:  $E_{\text{intra}} = (\text{EB}_5 - 16 \times \text{EB}_7 + \text{EB}_8) = -14.7 \text{ kJ mol}^{-1}$ . This corresponds to a considerable weakening in H-bonding relative to what was observed in crystalline ice polymorphs ( $E_{\text{HB}} \sim -22 \text{ kJ mol}^{-1}$ ).<sup>[10]</sup> One may think that this lower strength of the intramolecular H-bond energy might come from the occurrence of 12 intermolecular hydrogen bonds with the walls of the cavity. However, if one refers to Table 1, the order of magnitude of these interactions with the surface cavity can be estimated as  $\text{EB}_{\text{inter}} = (\text{EB}_4 - \text{EB}_2 + 2 \times \text{EB}_5) / 24 = -12.4 \text{ kJ mol}^{-1}$ . Consequently, the observed global weakening cannot be justified by the formation of stronger hydrogen bonds between the cluster and the cavity surface. It should then rather be associated to some intrinsic feature of the encapsulated cluster. At this stage, a further understanding requires a more detailed look into this interesting supramolecular architecture. Characterizing

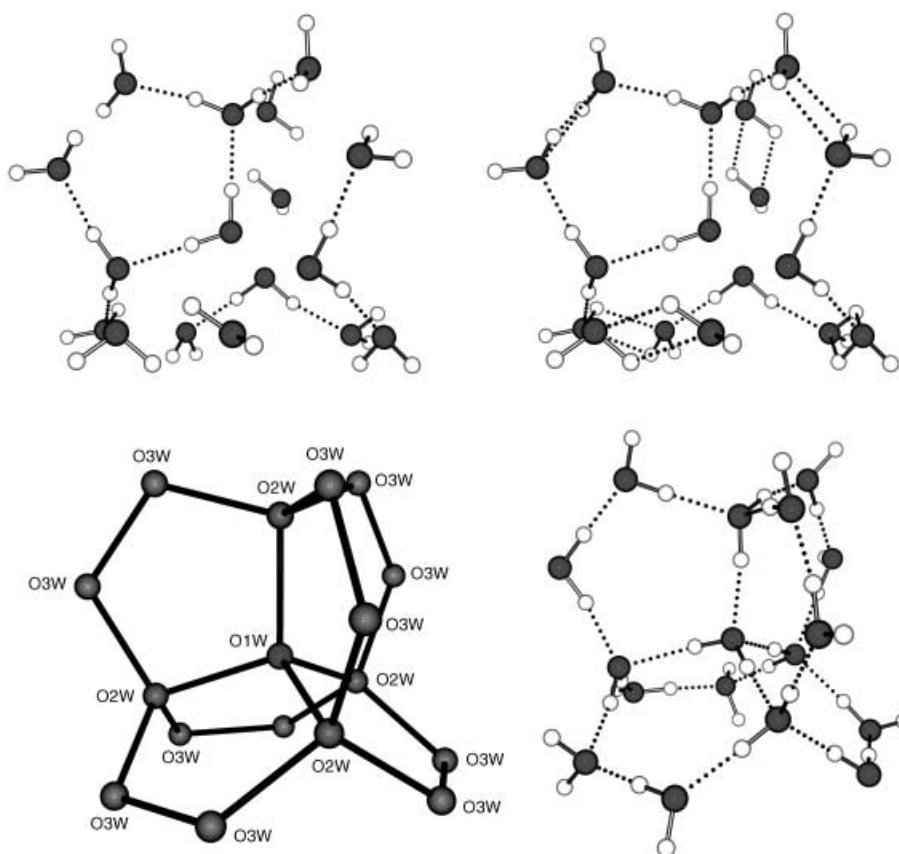


Figure 4. Predicted H-bond patterns for  $(\text{H}_2\text{O})_{17}$  water clusters that share the same metrical disposition of oxygen atoms: bottom left. Top left: pattern for the encapsulated cluster at 180 pm threshold showing four isolated water molecules, two linear trimers, and one branched heptamer. Top right: pattern at the 200 pm threshold that reveals unfavorable dimers. Bottom right: relaxed free  $(\text{H}_2\text{O})_{17}$  water cluster with its six pentagonal units spanning the edges of a central tetrahedron.

such an object by a single average value would obviously be far too restrictive.

The upper part of Figure 4 tries to unravel the supramolecular interactions at work that lead to the observed energy distribution. The top left drawing shows the H-bond pattern that emerges using a  $d[\text{H}\cdots\text{O}]_{\text{max}} = 180$  pm threshold for H-bond existence. At this level of significance, the cluster is found to break into four monomers, two linear trimers ( $\text{EB}_{10}$ ) and one branched heptamer made from two linear trimers ( $\text{EB}_{10}$ ) linked by the central water molecule. Hydrogen bonds within these four equivalent trimers ( $d_{\text{OO}} = 263$  pm) are found to be pretty strong:  $\text{EB}_{\text{trimer}} = (\text{EB}_{10} - (3 \times \text{EB}_7))/2 = -33.6 \text{ kJ mol}^{-1}$ . By contrast, the trimer ( $\text{EB}_{11}$ ) comprising the central water molecule and its two first neighbors at 276 pm has significantly weaker bonds:  $\text{EB}_{\text{trimer}} = (\text{EB}_{11} - (2 \times \text{EB}_7) - \text{EB}_8)/2 = -24.8 \text{ kJ mol}^{-1}$ . This explains the bimodal distribution observed for H bonds characterized by  $\theta(\text{H}-\text{O}\cdots\text{O}) < 5^\circ$ . At the 180 pm level of inference, we can then visualize a picture comprising four water molecules (ignoring the supramolecular water cluster) which prefer to bind with the wall of the cavity. At the center of the cavity, far from the walls, a central pivot water molecule is located, which exchanges ice-like hydrogen bonds with four very strongly associated trimers. It should be noted, however, that this convincing picture still does not explain

the strong weakening observed on average. The key feature is obtained by slightly increasing the significance threshold  $d[\text{H}\cdots\text{O}]_{\text{max}}$  at 200 pm (top right drawing of Figure 4). The immediate consequence is the appearance of six edge-sharing tetrahedral dimers characterized by quite short oxygen $\cdots$ oxygen distances (254 pm) associated to very weak interaction energies:  $\text{EB}_{\text{dim}} = (\text{EB}_9 - (2 \times \text{EB}_7))/2 = -11.4 \text{ kJ mol}^{-1}$ . This clearly demonstrates the amazing hierarchy—and complexity—that may arise in a system of H atoms interacting with quite a few oxygen atoms. Evidently, we are unveiling here a yet unsuspected property of the hydrogen bond: its ability to hide behind a standard average value ( $E_{\text{HB}} \sim -20 \text{ kJ mol}^{-1}$ ) two antagonist behaviors: weak interactions with  $E_{\text{HB}} \sim -10 \text{ kJ mol}^{-1}$  versus stronger ones characterized by  $E_{\text{HB}} < -30 \text{ kJ mol}^{-1}$ .

Referring back to Figure 4, we now readily anticipate that the naive pentagonal picture (bottom left) cannot be

reached by the H-bond network owing to the presence of the crystalline lattice. A further demonstration of this conclusion is provided by the consideration of the hydrogen-relaxed  $(\text{H}_2\text{O})_{17}$  water cluster. This new structure was obtained by exactly the same procedure as before, but after removal of all network atoms and after complete removal of translation symmetries (direct space finite summation instead of Madelung summation). As shown in Figure 4 (bottom right), the relaxed cluster displays 22 intramolecular hydrogen bonds, but in the form of six pentagonal  $(\text{H}_2\text{O})_5$  units spanning the six edges of a central  $(\text{H}_4\text{O})$  tetrahedron. This is exactly the naive structure that would have been expected in view of the O atoms disposition in the crystal. The mean H-bond energy associated with this new spatial disposition is evaluated from Table 1 as  $E_{\text{HB}} = (\text{EB}_{12} - (16 \times \text{EB}_7) - \text{EB}_{13})/22 = -36.3 \text{ kJ mol}^{-1}$ . Compared to crystalline ice, this is a fairly high value for an assembly of neutral molecules. Nevertheless, this cluster shares a common feature with ice networks, namely a pentameric tetrahedral unit  $(\text{H}_2\text{O})_5$ , which contains quite short O $\cdots$ O distances (276 pm here compared with 275 pm in ice  $I_h$ ). This allows us to check in a straightforward manner the consistency of our method by comparing the predicted H-bond energies for these two free pentameric units. As reported in Table 1, we obtain an  $E_{\text{penta}}$  value ( $E_{\text{penta}} = \text{EB}_{17} - (5 \times \text{EB}_7) = -26.4 \text{ kJ mol}^{-1}$ ) for the re-

laxed cluster that is very close to that obtained for the hexagonal ice network ( $E_{\text{penta}} = EB_{19} - (5 \times EB_{18}) = -24.5 \text{ kJ mol}^{-1}$ ). The small but significant difference observed is tentatively assigned to a higher stability of the pentagonal arrangement of water molecules versus the hexagonal one. It is therefore possible to conclude that the presence of translation symmetry operations in crystalline ices, by restricting the symmetries to the crystallographic ones only, limits the H-bond energy to values around  $-25 \text{ kJ mol}^{-1}$ . This readily explains why the water structure of the relaxed water cluster exhibits exceptional behavior in terms of the hydrogen bonding stabilization.

A comparison between both clusters (free versus encapsulated) is also very instructive. The most striking effect in the weakening of hydrogen bonds is the very large change in the distribution of  $\langle \text{O-H/O-O} \rangle$  angles. For the relaxed cluster all the H-bond angles are less than  $10^\circ$ , in contrast, in the encapsulated case 12 out of the 22 bonds display angles close to  $50^\circ$  (Figure 2). Relative to the relaxed case, which is characterized by a broad unimodal distribution centered at  $-40 \text{ kJ mol}^{-1}$ , the encapsulated cluster exhibits a shifted distribution of energies towards  $-20 \text{ kJ mol}^{-1}$ . The hydrogen bond network has therefore been “broken” by the constraints imposed on the cluster by the topology of the external hydrogen bonds with the inorganic interface. The match between the external geometry of the hydrogen bonds and the internal geometry cannot keep the average hydrogen bond energy at the same value for the encapsulated and the relaxed cluster. As both geometries clearly do not match, the cluster becomes frustrated compared to its relaxed state.

In the long-standing debate on the templating effect of organic cations for the nanoporous structures of zeolites and related materials, it is usually assumed that the shape constraints of the templating agent apply to the framework during formation (template imprinting). Zn-MIL-74 is a quite exceptional case. Usually, the templating effect associates the organic cation and its surrounding water, in a directing and shaping effect. In this case the cation is located in the inorganic framework, and the water molecules stay away from the cation, in the pore. For Zn-MIL-74, there is no cation inside the water cluster. Thus, in this case both structure-directing and shaping effects are independent. The shaping effect of the template onto the inorganic framework seems to be inverted. The inorganic framework imprints onto the water cluster its structure during the connecting process, if the water cluster can adapt it. In the present case, the conformational change associated with the inorganic framework formation is clearly monitored through the modification of the hydrogen bonds network. However, this water cluster does not have an infinite plasticity. This is the limit to the conformational change that the inorganic framework can impose onto the water cluster. This is most probably the central phenomenon of the shaping aspect of the templating effect: a bilateral effort between the inorganic framework and the templating agent to adapt to each other. Following this definition of the templating effect, the water cluster of Zn-MIL-74 possesses all the characteristics of a template.

The possibility for a H-bonding network to completely reorganize itself in response to a structural change has also far-reaching consequences in the field of molecular imprints. Accordingly, the development and use of molecular imprints, sometimes called “plastic antibodies”, is an emerging technology in which plastic impressions of a molecule are made by forming plastic polymers around a molecule and then extracting the molecule away leaving a newly formed polymer.<sup>[18–20]</sup> Our results strongly suggest that a crystalline framework is also able to imprint directly the polymeric structure of water. In the present case, the crystal has deposited its characteristic structural signature in the hydrogen network of the water cluster. Upon removal of the inorganic framework, a very stable  $(\text{H}_2\text{O})_{17}$  cluster forms by complete reorganization of its H-bond pattern. Owing to its very large bond energy ( $E_{\text{HB}} \sim -36 \text{ kJ mol}^{-1}$ ), if such a cluster could form spontaneously it would probably not be quickly destroyed by heating or by dilution with other water molecules so easily.

## Conclusion

In summary, it has been possible for the first time to fully quantify the various energetic interactions existing between a template molecule or a water cluster and the O atoms of a nanoporous inorganic framework. The lack of such an estimate stems from the scarcity of accurately located hydrogen atoms in the structure. The computed geometry and interaction energies obtained here are consistent with the assumptions made in usual estimates obtained from intuitive chemical knowledge:

- 1) Maximization of the number of hydrogen bonds between the template and the cavity walls.
- 2) Weaker N–H...O bonds relative to O–H...O bonds.
- 3) Weaker intermolecular O–H...O bonds relative to intramolecular ones.
- 4) Complete reorganization of the H-bond pattern after removal of the inorganic framework constraints upon the water cluster.

The plasticity of water molecules facing an inorganic framework during formation, accompanied by the large energetic gain due to the confined geometry, imprints some of the framework topological information onto the water cluster. The interplay between the water inside the crystal and the lattice energy can direct the structure formation towards a limited set of possible structures and its consideration may lead in template design to the elimination of some framework topologies that would not fit the water organization. This description matches the assumed role of water molecules in biological molecular recognition processes.

There are still many aspects to be thoroughly tested before this method of estimation may be systematically used for describing hydrogen-bonding networks. One of the main concerns is the fine-tuning of the numerical minimization procedures to avoid false minima while optimizing the positions of the hydrogen atoms. This requires a detailed evalua-

tion of hydrogen positioning versus neutron diffraction or NMR data as explained in reference [9].

- 
- [1] L. Beitone, C. Huguenard, A. Gansmüller, M. Henry, F. Taulelle, T. Loiseau, G. Férey, *J. Am. Chem. Soc.* **2003**, *125*, 9102
- [2] G. Férey, *J. Solid State Chem.* **2000**, *152*, 37.
- [3] M. O'Keeffe, M. Eddaoudi, H. Li, T. Reineke, O. Yaghi, *J. Solid State Chem.* **2000**, *152*, 3.
- [4] R. M. Barrer, *Hydrothermal Chemistry of Zeolites*, Academic Press, London, **1982**.
- [5] H. Gies, B. Marler, *Zeolites* **1994**, *12*, 42.
- [6] S. L. Lawton, W. J. Rohrbaugh, *Science* **1990**, *247*, 1319.
- [7] G. Cheetham, M. M. Harding, *Zeolites* **1996**, *16*, 245.
- [8] D. W. Lewis, C. M. Freeman, C. R. A. Catlow, *J. Phys. Chem.* **1995**, *99*, 11 194.
- [9] M. Henry, *Chem. Phys. Chem.* **2002**, *3*, 561.
- [10] M. Henry, *Chem. Phys. Chem.* **2002**, *3*, 607.
- [11] R. P. Feynman, *Phys. Rev.* **1939**, *56*, 340.
- [12] J. Dore, *Chem. Phys.* **2000**, *258*, 327.
- [13] J. Teixeira, J.-M. Zanotti, M.-C. Bellissent-Funel, S.-H. Chen, *Physica B+C* **1997**, *370*, 234–236.
- [14] K. Liu, M. G. Brown, C. Carter, R. J. Saykally, J. K. Gregory, D. C. Clary, *Nature* **1996**, *381*, 501.
- [15] J. M. Ugalde, I. Alkorta, J. Elguero, *Angew. Chem.* **2000**, *112*, 733; *Angew. Chem. Int. Ed.* **2000**, *39*, 717.
- [16] R. Ludwig, *Angew. Chem.* **2001**, *113*, 1856; *Angew. Chem. Int. Ed.* **2001**, *40*, 1809.
- [17] L. Beitone, J. Marrot, T. Loiseau, G. Férey, M. Henry, C. Huguenard, A. Gansmüller, F. Taulelle, *J. Am. Chem. Soc.* **2003**, *125*, 1912.
- [18] G. Vlatakis, L. I. Andersson, R. Müller, K. Mosbach, *Nature* **1993**, *361*, 645.
- [19] F. Flame, *Science* **1994**, *263*, 1221.
- [20] F. L. Dickert, P. Lieberzeit, M. Tortschanoff, *Sens. Actuators, B* **2000**, *65*, 186.

Received: May 15, 2003  
Revised: September 1, 2003 [F5143]